Monthly Notices
of the
ROYAL ASTRONOMICAL SOCIETY

MNRAS **500,** 4439–4447 (2021)
Advance Access publication 2020 November 18

doi:10.1093/mnras/staa3525

Accelerating computation of the density-field filtering scale $\sigma(R)$ and non-linear mass by an order of magnitude

Alex Krolewski[1,2]★ and Zachary Slepian[1,3]

[1] *Lawrence Berkeley National Laboratory, 1 Cyclotron Road, Berkeley, CA 94720, USA*
[2] *Berkeley Center for Cosmological Physics, University of California, Berkeley, Berkeley, CA 94720, USA*
[3] *Department of Astronomy, University of Florida, 211 Bryant Space Science Center, Gainesville, FL 32611, USA*

Accepted 2020 November 7. Received 2020 November 7; in original form 2019 November 27

ABSTRACT

The non-linear mass is a characteristic scale in halo formation that has many applications across cosmology. Naively, computing it requires repeated numerical integration to calculate the variance of the power spectrum on different scales and determine which scales exceed the threshold for non-linear collapse. We accelerate calculation of both the non-linear mass and the rms amplitude of the power spectrum $\sigma(R)$ by working in configuration space and approximating the correlation function as a polynomial at $r \leq 5\ h^{-1}$ Mpc. This enables an analytic rather than numerical solution for the non-linear mass, accurate across a variety of cosmologies to 0.1–1 per cent in mass (depending on redshift) and 20–60× faster than the standard numerical method. We also present a further acceleration of the non-linear mass (400–1000× faster than the standard method) in which we determine the polynomial coefficients using a Taylor expansion in the cosmological parameters rather than re-fitting a polynomial to the correlation function. Our method is also 500× faster than the standard method for $\sigma(R)$ for a typical case of $N_R = 100$ desired R values, with timing essentially independent of N_R. Our approach can be used for quick calculation of the halo mass function, halo mass–bias relation, and cosmological calculations involving the non-linear mass.

Key words: methods: numerical – cosmology: theory.

1 INTRODUCTION

Computing the spatial scale on which the density fluctuations have variance of order unity is a common problem in cosmology. In bottom-up structure formation, fluctuations are small on large scales and become progressively larger on smaller scales. As the density fluctuations approach unity, perturbation theory (PT)-plus-biasing-based models of the clustering (Bernardeau et al. 2002) break down, and density fluctuations begin to collapse into dark matter haloes.

The non-linear scale $R_{\rm NL}$ is the characteristic scale at which these processes occur. Its technical definition is the scale at which the rms of the density field fluctuations, σ_R, reaches $\delta_c = 1.686$ (Bryan & Norman 1998; Child et al. 2018), the linear-density threshold for spherical tophat collapse in an Einstein de-Sitter universe (Gunn & Gott 1972); in a Λ cold dark matter (ΛCDM) universe, δ_c has a very mild dependence on cosmological model and halo formation redshift (Lacey & Cole 1993; Eke, Cole & Frenk 1996; Nakamura & Suto 1997; Mead 2017), which we neglect in this work. The non-linear scale $R_{\rm NL}$ can also be converted into a non-linear mass $M_{\rm NL}$ by multiplying by the background density $\rho_{\rm bgd}$.[1]

The non-linear mass depends weakly on cosmology, with the cosmology dependence arising from the small-scale power spectrum. Beyond the dependence on the amplitude σ_8 and the spectral slope n_s, $R_{\rm NL}$ is most sensitive to Ω_m. Increasing Ω_m decreases the elapsed time in radiation domination. This leads to less suppression of small-scale modes entering the horizon during radiation domination, ultimately increasing small-scale power. The small-scale power spectrum is also sensitive to Ω_b, both because baryons slow the growth of structure after matter-radiation equality but before decoupling (equation E-6 in Hu & Sugiyama 1996), and because the baryonic Jeans scale suppresses power at $k \geq 300\ h\ {\rm Mpc}^{-1}$.

The non-linear mass has broad applications across cosmology. Most importantly, it is the characteristic scale of halo formation in a scale-free power-law cosmology (Kravtsov & Borgani 2012) and is consequently the characteristic mass scale for self-similar scaling relations in galaxy clusters (Kaiser 1986; Bryan & Norman 1998; Norman 2010; Kravtsov & Borgani 2012). Although the non-linear mass is not exactly the characteristic halo mass scale in a ΛCDM power spectrum, it is a good enough approximation that deviations from self-similar scalings are often parametrized in terms of it (Kravtsov & Borgani 2012). As an important determinant of halo formation, the non-linear mass is the key scale in the halo growth rate (Wechsler et al. 2002), the concentration–mass relation (Child et al. 2018), assembly bias (Dalal et al. 2008), the mass–bias relation (Seljak & Warren 2004), and spin alignment between haloes and filaments (Hahn et al. 2007a,b).

Due to these broad applications, the non-linear mass plays a role in modelling non-linear structure growth via the halo model (Ma & Fry

★ E-mail: krolewski@berkeley.edu, akrolews@uwaterloo.ca (AK); zslepian@ufl.edu (ZS)

[1] The background density may be either the matter density or the critical density, but does not contain a factor of $\Delta_c \sim 200$, the final-state overdensity of a virialized halo. This is because the non-linear mass is defined with reference to the *linear* density threshold for the initial conditions of collapse.

© 2020 The Author(s)
Published by Oxford University Press on behalf of the Royal Astronomical Society

Downloaded from https://academic.oup.com/mnras/article/500/4/4439/5989726 by guest on 24 April 2024

2000; Abazajian et al. 2005; Cataneo et al. 2020) and parametrizing the halo mass function to obtain σ_8 (Seljak et al. 2005). The non-linear mass appears in the scale-dependent bias model of Jose, Lacey & Baugh (2016), which has been used to model the clustering of high-redshift galaxies (Jose et al. 2017; Harikane et al. 2018). The non-linear mass also appears in fitting formulae for the triaxiality of haloes (Jing & Suto 2002). These formulae have in turn provided priors on haloes' axial ratios when fitting strong lensing data (Oguri et al. 2005). The non-linear mass features in cosmological constraints from the highly non-linear regime, including weak lensing halo mass profiles (Umetsu et al. 2020) and cluster abundances (Bocquet et al. 2019). For instance, in the baryon-feedback model of Mead et al. (2015), which is included in the KiDS weak lensing analysis (Hildebrandt et al. 2020), the amplitude of feedback depends on the mass–concentration relation. While the mass–concentration relation of Bullock et al. (2001) used by Mead et al. (2015) does not depend on the non-linear mass, other mass–concentration relations do (Child et al. 2018), so modified feedback models generically can involve the non-linear mass.

We now outline how one might naively calculate the non-linear mass, explain why this is inefficient, and sketch this work's approach to accelerate the calculation of both the non-linear mass and of σ_R. In the standard method, one computes a numerical integral for σ_R at each point in R traversed by a numerical root-finder solving the equation $\sigma_R = \delta_{\rm c}$. The combination of the numerical integration and the root-finding makes $R_{\rm NL}$ slow to calculate.

In this work, we present a scheme to greatly accelerate calculation of the non-linear mass and σ_R. Our method uses the algebraic solution of a cubic equation to determine $R_{\rm NL}$, thereby bypassing both the numerical integration and the root-finding. In particular, we work in configuration space and fit a polynomial to the correlation function on small scales. σ_R is a compactly supported integral over the correlation function, so these fitted coefficients immediately give us the integral's value as a cubic in $R_{\rm NL}$. The equation $\sigma_R = \delta_{\rm c}$ can then be solved analytically. Our method is accurate to <1 per cent on the non-linear mass for a variety of cosmologies, an order of magnitude faster than the standard method, and can be further accelerated by an additional order of magnitude using a Taylor series to determine the polynomial coefficients of the correlation function. It is also 500× faster than the standard method for computing σ_R for a typical case of 100 desired R values, and is therefore also useful for quick calculations of the halo mass function and halo mass–bias relation.

All numerical work in this paper uses the best-fitting cosmology from the *Planck* 2018 release (Planck Collaboration et al. 2020) with $\Omega_{\rm m} = 0.3096$, $\Omega_{\rm b} = 0.04897$, $n_{\rm s} = 0.9665$, $\sigma_8 = 0.8102$, $m_\nu = 0.06$ eV and $h = 0.6766$.[2] Consistent with past work (e.g. Child et al. 2018), we use the linear power spectrum of cold dark matter plus baryons, since haloes do not respond to neutrinos (Costanzi et al. 2013; Castorina et al. 2014, 2015; Villaescusa-Navarro et al. 2014). Our PYTHON code is publicly available.[3]

2 METHOD AND IMPLEMENTATION

In this section, we review the calculation of the variance of the density field in Section 2.1, present our algebraic method in Section 2.2, and show the solution to the cubic in Section 2.3.

2.1 Variance of the density field

The variance of the linear density field at a point $\vec{x}$ and redshift z within a sphere of radius R is

$$\sigma_R^2(\vec{x}, z) = V_R^{-2} \int {\rm d}^3\vec{r}\ {\rm d}^3\vec{r}'\ \Theta(R - |\vec{r}|)\Theta(R - |\vec{r}'|)\delta_{\rm lin} \times (\vec{x} + \vec{r}, z)\delta_{\rm lin}(\vec{x} + \vec{r}', z). \tag{1}$$

Note that this expression is equivalent to writing $\vec{x} - \vec{r}$ and $\vec{x} - \vec{r}'$ as the arguments of $\delta_{\rm lin}$, since the minus signs from the transformations from $\vec{r}$ to $-\vec{r}$ and $\vec{r}'$ to $-\vec{r}'$ would cancel each other out. Θ is a Heaviside function, unity where its argument is positive and zero otherwise. In 3D, the Heaviside function of radius is simply a spherical tophat. $V_R = 4\pi R^3/3$ is the volume of a sphere of radius R.

The statistical homogeneity of the density field implies translation invariance, and we may therefore write the average over $\vec{x}$ as

$$\begin{aligned}\sigma_R^2(z) &\equiv \left\langle \sigma_R^2(\vec{x}, z)\right\rangle = \frac{1}{V}\int {\rm d}^3\vec{x}\ \sigma_R^2(\vec{x}, z)\\ &= V_R^{-2}\int {\rm d}^3\vec{r}\ {\rm d}^3\vec{s}\ \Theta(R - |\vec{r}|)\Theta(R - |\vec{r} + \vec{s}|)\xi(s, z),\end{aligned} \tag{2}$$

where $\vec{s} = \vec{r}' - \vec{r}$, with ξ is the *linear* matter correlation function:

$$\begin{aligned}\xi(s, z) &\equiv \int {\rm d}^3\vec{x}\ \delta_{\rm lin}(\vec{x} + \vec{r}, z)\ \delta_{\rm lin}(\vec{x} + \vec{r} + \vec{s}, z)\\ &= \int {\rm d}^3\vec{x}\ \delta_{\rm lin}(\vec{x}, z)\ \delta_{\rm lin}(\vec{x} + \vec{s}, z)\end{aligned} \tag{3}$$

and $\delta_{\rm lin}$ is the linear density field. The equality in the second line follows by change of integration variable. To obtain the second equality in equation (2), we inserted equation (1) for $\sigma_R(\vec{x}, z)$ and integrated over ${\rm d}^3\vec{x}$, first using the definition of ξ in equation (3). By recasting equation (2) as a convolution we obtain

$$\sigma_R^2(z) = V_R^{-2}\int {\rm d}^3\vec{s}\ \xi(s, z)\,[\Theta(R) \star \Theta(R)]\,(\vec{s}), \tag{4}$$

where 'star' denotes convolution.[4] The convolution inside the square brackets is evaluated at an offset $\vec{s}$ and is itself an integral over the dummy variable $\vec{r}$; for clarity we have suppressed this latter argument. Equation (4) shows that the variance is thus just the integral of the correlation function against a kernel given by the convolution of two spherical tophats at an offset $\vec{s}$.

The overlap of the two spheres forms a lens. Consequently, we can evaluate the convolution using the formula for the volume of a lens produced by overlapping two spheres of radius R, offset from each other by s:[5]

$$[\Theta(R) \star \Theta(R)]\,(\vec{s}) = V_{\rm lens}(s; R) = \frac{\pi}{12}(4R + s)(2R - s)^2. \tag{5}$$

In the limit $s \to 0$, i.e. when the two spheres share a common centre, this expression recovers the volume of a sphere.

Inserting equation (5) in equation (4) yields

$$\begin{aligned}\sigma_R^2(z) &= 4\pi V_R^{-2}\int_0^{2R} s^2{\rm d}s\ \xi(s, z)V_{\rm lens}(s; R)\\ &= \frac{\pi^2}{3}V_R^{-2}\int_0^{2R} s^2{\rm d}s\ \xi(s, z)(4R + s)(2R - s)^2\\ &= \frac{\pi^2 R^3}{3V_R^2}\int_0^{2} y^2{\rm d}y\ \xi(yR, z)(4R + yR)(2R - yR)^2.\end{aligned} \tag{6}$$

[2] If one computes σ_8 using our fiducial CDM-plus-baryons $P(k)$, one obtains 0.8138, in contrast to the *Planck* value of 0.8102, which is calculated for $P(k)$ including CDM, baryons and neutrinos.

[3] https://github.com/akrolewski/NonlinearMassFaster

[4] This formula offers a geometric way to show that the overlap integral of two spherical Bessel functions $j_1(kR)j_1(ks)$ scales as the volume of the lens formed by the overlap of two spheres.

[5] https://mathworld.wolfram.com/Sphere-SphereIntersection.html

Downloaded from https://academic.oup.com/mnras/article/500/4/4439/5989726 by guest on 24 April 2024

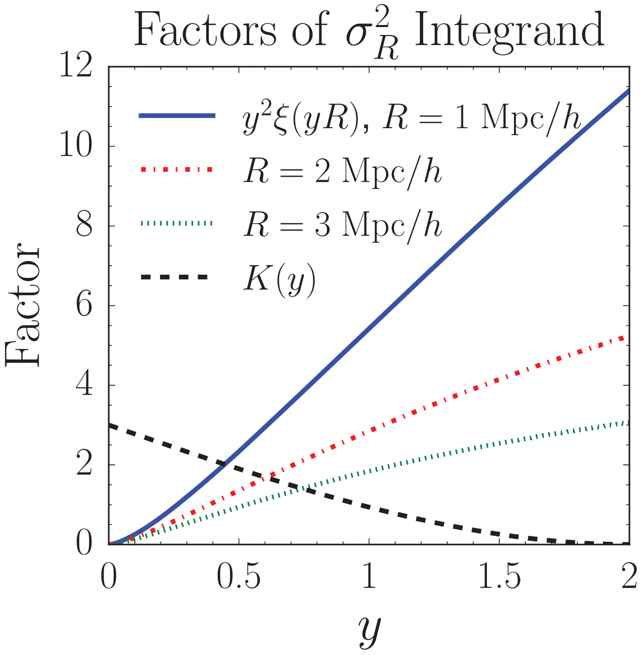

Figure 1. Different pieces of the integral (7). The dashed black line is the kernel *K(y)* defined in equation (8); and the short-dashed, dot–dashed, and solid lines (various colours) are $y^2\xi(yR)$ at $R = 1, 2$, and 3 Mpc/*h*. The dominant contribution to σ_R^2 comes from intermediate *y*, where both *K*(*y*) and $y^2\xi(yR)$ are non-zero.

To obtain the third equality we changed variables to $s = yR$, $s^2\mathrm{d}s = R^3y^2\mathrm{d}y$. Simplifying the last line we obtain the formula of Zehavi et al. (2005), quoted there without proof but obtained by direct integration:[6]

$$\sigma_R^2(z) = \int_0^2 \mathrm{d}y\ y^2\ \xi(yR, z)\ K(y), \tag{7}$$

with

$$K(y) = \left(3 - \frac{9y}{4} + \frac{3y^3}{16}\right). \tag{8}$$

We will refer to *K*(*y*) as defined in equation (8) as the 'kernel' for the remainder of this work. We plot the components of equation (7) in Fig. 1, including the kernel and $y^2\xi(yR, z = 0)$ for different values of *R*. Since *K*(*y*) is nearly zero at $y > 1.5$ and $y^2\xi(yR)$ is nearly zero at $y < 0.5$, much of the integral comes from intermediate values of *y*.

2.2 Solving for the non-linear scale

The standard approach to computing R_{NL} is to use the convolution theorem to perform the convolution (equation 4) as a product in Fourier space, i.e.

$$\sigma_R^2(z) = \int \frac{k^2\mathrm{d}k}{2\pi^2}\left[\frac{3j_1(kR)}{kR}\right]^2 P(k, z), \tag{9}$$

where the quantity in square brackets is the square of the Fourier transform of a spherical tophat. One would then use numerical root-finding to solve the equation $\sigma_{R_{\mathrm{NL}}}(z) = \delta_c = 1.686$. In this paper we take δ_c to be a redshift and cosmology-independent constant.

In a non-EdS universe, δ_c has a mild dependence on cosmology and redshift, deviating less than 3 per cent from its EdS value (Mead 2017). Our method could be modified to account for this dependence. The redshift dependence of δ_c could be absorbed into *D*(*z*), and the cosmology dependence is small enough to be neglected. A change in the dark energy equation of state $\Delta w = 0.1$ changes δ_c ($z = 0$) by <0.5 per cent (using fig. A1 of Mead 2017 to convert Δw to an approximate change in δ_c). For many applications, one could thus neglect the cosmology dependence of δ_c entirely.

A more substantial change is to define the non-linear scale as $\sigma_{R_{\mathrm{NL}}}(z) = 1$ (Norman 2010), which will clearly require recomputation of R_{NL}. As discussed in Section 4, we expect that our method is slightly more accurate for the choice that $\sigma_{R_{\mathrm{NL}}}(z) = 1$ than for the choice that $\sigma_{R_{\mathrm{NL}}}(z) = 1.686$, because R_{NL} has weaker cosmology-dependence for smaller δ_c, in turn allowing us to choose a more appropriate fitting range that leads to a better polynomial approximation.

Our method evaluates σ_R^2 from equation (7) in configuration space and fits a low-order polynomial to the small-scale correlation function, leading to an analytic integral that enables algebraic calculation of R_{NL}. This is an order of magnitude faster than the standard method to compute R_{NL} from numerical integrals of the power spectrum.

Our method offers two advantages that substantially accelerate the calculation of the non-linear scale. First, the configuration space integral is easier to handle than the Fourier space integral, which has an infinite upper bound and BAO wiggles that require a larger number of *k* steps for accurate sampling. Secondly, the correlation function on small scales is smooth and can be approximated by a low-order polynomial (Fig. 2). This allows the σ_R^2 integral to be evaluated analytically and R_{NL} then computed algebraically.

To obtain an analytic expression for σ_R^2 for a polynomial correlation function, we start with the middle line in equation (6); separating the integrals term by term we find

$$\sigma_R^2(z) = \mathrm{D}^2(z)\ R^{-3}\left\{3\int_0^{2R}\mathrm{d}s\ s^2\xi(s) - \frac{9}{4R}\int_0^{2R}\mathrm{d}s\ s^3\xi(s)\right.$$
$$\left. + \frac{3}{16R^3}\int_0^{2R}\mathrm{d}s\ s^5\xi(s)\right\}, \tag{10}$$

where we explicitly separate the redshift-dependent piece of the linear correlation function, the square of the linear growth factor $D^2(z)$, and hereafter use $\xi(s)$ to mean $\xi(s, z = 0)$. We use the small-scale limit of the linear growth factor appropriate for a massive neutrino cosmology with $m_\nu = 0.06$ eV (Hu & Eisenstein 1998). While growth is scale-dependent in a massive neutrino cosmology, the scales relevant to the non-linear mass are much smaller than the neutrino free-streaming scale. Thus the effect of neutrinos on these scales is very nearly a constant rescaling. As a result, separating the scale and redshift-dependence of *P*(*k*, *z*) is a very good approximation.

We perform the integral in equation (10) analytically by expanding $s^2\xi(s)$ as a polynomial:

$$s^2\xi(s) = \sum_{n=0}^{n_{\max}} c_n s^n. \tag{11}$$

We chose a polynomial because it allows the integral in equation (7) to be done analytically and provides a good fit to the correlation function over the restricted range required ($s \leq 5\ h^{-1}$ Mpc).

Inserting the expansion (11) into equation (10) and performing the integrals, we obtain the following expression for σ_R^2, which we set

[6] D. Eisenstein (private communication).

Downloaded from https://academic.oup.com/mnras/article/500/4/4439/5989726 by guest on 24 April 2024

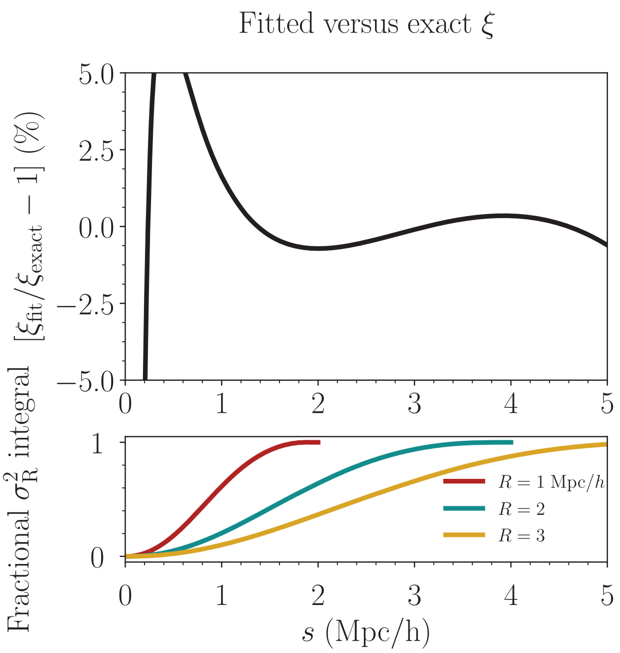

Figure 2. Top: Difference between $s^2\xi_{\rm lin}(z = 0)$ and the third-order polynomial fit to it. The differences in fitting quality are negligible among different cosmologies. We recover the exact correlation function to rather high accuracy, generally sub per cent over most of its domain; larger errors occur at small scales which contribute little to the fractional σ^2_R integral, as shown in the bottom panel. Bottom: Fractional buildup of σ^2_R (equation 7) as a function of $s \equiv yR$. Since the integral extends to $y = 2$, the curves cut off at respectively $yR = 2, 4$, and 6 for $R = 1$, 2, and 3 Mpc h^{-1}. For a wide range in R, the integral turns out to be most sensitive to exactly the region in which our fit performs best, $1 < s < 5\,h^{-1}$ Mpc.

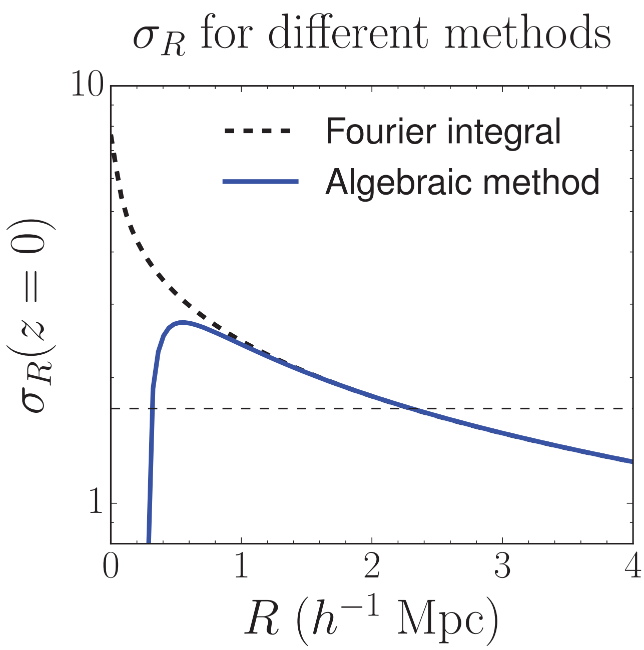

Figure 3. Comparison between exact σ_R from the Fourier integral (blue; equation 9) and our algebraic method (black; equation 14). Both calculations are done at $z = 0$; results for $\sigma_R(z)$ will be very similar, except that the horizontal axis will be scaled by $R_{\rm NL,fid}(z)/R_{\rm NL,fid}(z = 0)$. The thin black dashed line gives $\sigma_R = \delta_{\rm c} = 1.686$; thus, $R_{\rm NL}$ is where the thicker curves cross the dashed line. While the solid and dashed curves disagree at small scales, the agreement is almost perfect near where $\sigma_R = 1.686$.

equal to $\delta^2_{\rm c}$:

$$\begin{aligned}\sigma^2_{R_{\rm NL}}(z) = D^2(z)\sum_{n=0}^{n_{\rm max}} c_n R_{\rm NL}^{-3}\left\{3\,\frac{2^{n+1}}{n+1}R_{\rm NL}^{n+1} - \frac{9}{4R_{\rm NL}}\,\frac{2^{n+2}}{n+2}R_{\rm NL}^{n+2}\right. \\ \left. + \frac{3}{16R^3_{\rm NL}}\,\frac{2^{n+4}}{n+4}R_{\rm NL}^{n+4}\right\} \\ = D^2(z)\sum_{n=0}^{n_{\rm max}} 2^{n+1}c_n R_{\rm NL}^{n-2}\left\{\frac{9}{n^3+7n^2+14n+8}\right\} = \delta^2_{\rm c}.\end{aligned} \qquad (12)$$

We transform equation (12) from a sum of inverse powers to a polynomial by multiplying through by $R^2_{\rm NL}$:

$$\frac{R^2_{\rm NL}\delta^2_{\rm c}}{D^2(z)} = \sum_{n=0}^{n_{\rm max}} 2^{n+1}c_n R^n_{\rm NL}\left\{\frac{9}{n^3+7n^2+14n+8}\right\}. \qquad (13)$$

This is an order-$n_{\rm max}$ polynomial in $R_{\rm NL}$. Quartics and lower-order polynomials have a closed form solution, but quintics and higher-order polynomials do not (this is known as the Abel–Ruffini theorem). Therefore, if $n_{\rm max} \le 4$, we can solve in closed form for $R_{\rm NL}$.

We find that $n_{\rm max} = 3$ is sufficient to reproduce $s^2\xi(s)$ to per cent-level accuracy (Fig. 2), implying that an algebraic solution for $R_{\rm NL}$ exists. While Fig. 2 only shows the fit to the correlation function in the *Planck* 2018 cosmology, $s^2\xi(s)$ can be approximated equally well by a cubic across a wide range of cosmologies. Because the cubic provides a good fit across a wide range in s, the analytic approximation of σ_R from integrating equation (10) provides a very good match to the numerical solution from the Fourier-space integral at $R > 0.5\,h^{-1}$ Mpc at $z = 0$ (Fig. 3).

We found that the cubic provides the best balance between simplicity and accuracy: a quadratic approximation is considerably less accurate, whereas a quartic offers only minimal improvement. Other possibilities, such as omitting the constant and linear terms or requiring the constant term to be positive, degrade the accuracy of the fit. While a piecewise function (e.g. a smoothing spline) can reproduce $s^2\xi(s)$ to arbitrary accuracy, the upper bounds in the integrals in equation (10) are no longer linear multiples of R, and thus contribute an R^{-6} term in equation (12). If $n_{\rm max} \ge 1$, this yields a fifth-order polynomial with no analytic solution in equation (14).

Equation (11) must approximate $s^2\xi(s)$ well at $s < 2R_{\rm NL}(z)$, since this is the upper bound of the integral in equation (10). To avoid the circularity of requiring $R_{\rm NL}$ to fit the c_n, we fit the c_n to $s < 1.9R_{\rm NL,fid}(z)$, where $R_{\rm NL,fid}$ is $R_{\rm NL}$ in the fiducial *Planck* 2018 cosmology. We empirically find that using an upper cutoff of $1.9R_{\rm NL,fid}(z)$ leads to 20 per cent better accuracy than using $2R_{\rm NL,fid}(z)$. This slightly up-weights smaller and intermediate scales that contribute more to the σ^2_R integral (bottom panel of Fig. 2).

Allowing the fitting range (and thus the c_n) to vary in redshift is critical, because the error on the cubic increases greatly at small s: this is the sharp drop in the signed deviation between the correlation function and the cubic fit at $s \le 0.5\,h^{-1}$ Mpc in Fig. 2 (or equivalently, the downturn in σ^2_R at $R > 1\,h^{-1}$ Mpc in Fig. 3). If we calculated $R_{\rm NL}(z = 6)$ using $c_n(z = 0)$, we would be primarily using scales where the cubic provides an extremely poor fit to $s^2\xi(s)$, leading to a severe loss of accuracy. Instead, we fit over a very restricted s range at $z = 6$, ensuring an accurate fit over the vast majority of the relevant range in s. Because of this rescaling in $R_{\rm NL,fid}(z)$, Figs 2 and 3 at $z =$

Downloaded from https://academic.oup.com/mnras/article/500/4/4439/5989726 by guest on 24 April 2024

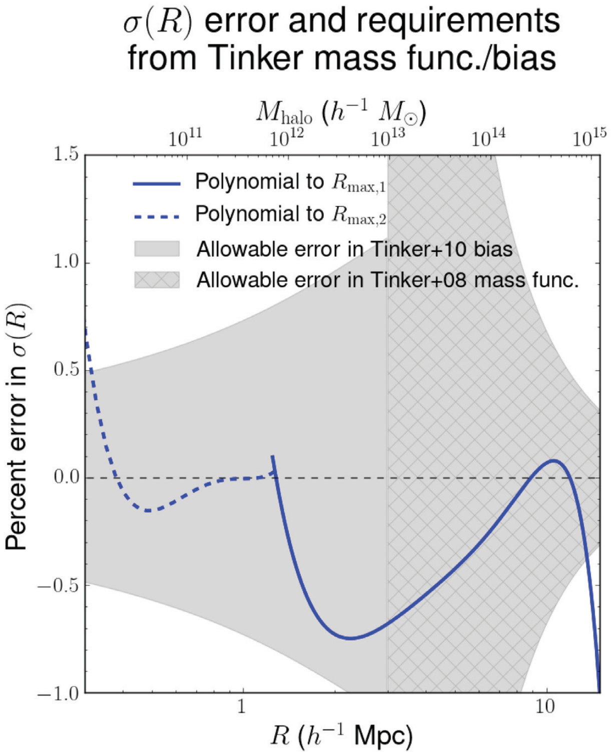

Figure 4. Our method can also be used for very fast calculations of the halo mass function and mass–bias relation, since it accelerates the computation of $\sigma(R)$, a major bottleneck in these calculations. The blue curve shows the per cent error on $\sigma(R)$ from the polynomial fit to the correlation function. To ensure accuracy across a sufficiently wide range in mass, the polynomial in the correlation function is piecewise (solid and dashed curves). The grey region (grey hatched region) shows the allowable error in the mass function (mass–bias relation) of Tinker et al. (2008, 2010), corresponding to half of the statistical scatter of simulation results about these relations.

0 are very similar to the equivalent figures at high redshift, except that the s (R) axis will be rescaled by $R_{\rm NL,fid}(z)/R_{\rm NL,fid}(z=0)$.

Our method can also be used for quick and accurate calculations of $\sigma(R)$, which in turn informs the halo mass function (Tinker et al. 2008) and the halo mass–bias relationship (Tinker et al. 2010). Here the relevant range of scales is larger than for the non-linear mass: halo masses of 10^{10}–10^{15} h^{-1} M$_\odot$ correspond to radii of 0.3–14.2 h^{-1} Mpc. We therefore fit the polynomial coefficients out to $R_{\rm max,1} = 30$ h^{-1} Mpc.

At small scales, the polynomial approximation breaks down (the turnover in Fig. 3), and for $R < 1.32$ h^{-1} Mpc, we therefore fit a second set of polynomial coefficients with $R_{\rm max,2} = 2.0$ h^{-1} Mpc. $R_{\rm max,2}$ is determined by the accuracy tolerance on $\sigma(R)$. In turn, the $\sigma(R)$ accuracy requirement comes from the desired accuracy on the bias or halo mass function. The fitting function of Tinker et al. (2010) is accurate to 6 per cent for the bias, and the fitting function of Tinker et al. (2008) is accurate to 5 per cent for the halo mass function. Therefore, we require that our method adds additional errors of 3 per cent in the bias and 2.5 per cent in the mass function, such that the quadrature sum of the fitting error from Tinker et al. (2008, 2010) and from our method is nearly the same as the fitting error. We compute the derivatives of bias and number density with respect to σ for halo density contrast $\Delta = 200$ and $z = 0$ (our results are nearly the same at the highest redshift considered, $z = 6$). We then use error propagation to convert from error on bias or mass function to error on $\sigma(R)$. In Fig. 4, we show that our scheme achieves sufficient accuracy at $0.32 < R < 13.65$ h^{-1} Mpc, or equivalently $1.19 \times 10^{10} < M < 9.05 \times 10^{14}$ h^{-1} M$_\odot$.

2.3 Detailed solution of the cubic

In this section, we explicitly show how one obtains $R_{\rm NL}$ algebraically. Evaluating equation (13) with $n_{\rm max} = 3$ yields

$$\frac{9}{4}R^{-2}c_0 + \frac{6}{5}R^{-1}c_1 + c_2 + \frac{36}{35}R\,c_3 = \frac{\delta_{\rm c}^2}{D^2(z)}. \quad (14)$$

To simplify what follows, we define coefficients a_i that incorporate both the c_n and their numerical pre-factors in equation (14), as

$$a_0 = \frac{9c_0}{4}, \quad a_1 = \frac{6c_1}{5}, \quad a_2 = c_2, \quad a_3 = \frac{36c_3}{35}. \quad (15)$$

We now rewrite equation (14) in standard cubic form

$$R^3 + \alpha_2 R^2 + \alpha_1 R + \alpha_0 = 0 \quad (16)$$

with the α_i given as

$$\alpha_0 = \frac{a_0}{a_3}, \quad \alpha_1 = \frac{a_1}{a_3}, \quad \alpha_2 = \frac{a_2 - 1/D(z)^2}{a_3}. \quad (17)$$

We can obtain the solution using Cardano's formula for the cubic.[7] We find the roots R_i as:

$$\begin{aligned} R_1 &= -\frac{1}{3}\alpha_2 + (S+T), \\ R_2 &= -\frac{1}{3}\alpha_2 - \frac{1}{2}(S+T) + \frac{1}{2}i\sqrt{3}(S-T), \\ R_3 &= -\frac{1}{3}\alpha_2 - \frac{1}{2}(S+T) - \frac{1}{2}i\sqrt{3}(S-T). \end{aligned} \quad (18)$$

We define the auxiliary variables Q, R, D, S, and T as

$$Q \equiv \frac{3\alpha_1 - \alpha_2^2}{9}, \quad R \equiv \frac{9\alpha_2\alpha_1 - 27\alpha_0 - 2\alpha_2^3}{54},$$
$$D \equiv Q^3 + R^2, \quad S \equiv \sqrt[3]{R + \sqrt{D}}, \quad T \equiv \sqrt[3]{R - \sqrt{D}}. \quad (19)$$

We choose the real and positive root. Note that despite the presence of i in R_2 and R_3, they need not be complex because S and T are also complex and can render the factor involving i real overall.

3 NUMERICAL IMPLEMENTATION

To obtain the non-linear scale using the method outlined in Sections 2.2 and 2.3, we first need the linear correlation function. We obtain the correlation function by transforming the linear power spectrum from CAMB (Lewis, Challinor & Lasenby 2000; Howlett et al. 2012).[8] We use 800 logarithmically spaced sample points per decade over the range $k = 10^{-3}$ to 10^4 h Mpc^{-1}. We use the FFTLog (Hamilton 2000) algorithm (as implemented in MCFIT;[9] Li 2019) to transform from $P(k)$ to $\xi(s)$, and then linearly interpolate between the resulting sampling points in s. For consistency with past work (Child et al. 2018), we use the power spectrum of baryons plus CDM in our numerical implementation, but the method is general and can accept an arbitrary linear power spectrum as input.

[7] https://mathworld.wolfram.com/CubicFormula.html
[8] http://camb.info
[9] https://github.com/eelregit/mcfit

Downloaded from https://academic.oup.com/mnras/article/500/4/4439/5989726 by guest on 24 April 2024

The most time-consuming part of our implementation of the polynomial method is solving for the polynomial coefficients c_n. We use 1000 sampling points for the correlation function and determine c_n via linear least-squares. The relevant operations are vectorized so the performance is not highly sensitive to the number of sampling points. Consequently, we can choose 1000 points to preserve accuracy yet not pay much price in speed. The rate-limiting step is matrix inversion in the linear least-squares fitting; to speed this up, we take advantage of the fact that the relevant matrix is symmetric, as it is the product of the Vandermonde matrix and its transpose. We solve the least-squares equation using the LAPACK linear algebra package routine DPOTRS (**d**ouble-precision **po**sitive **tr**iangular matrix **s**olve), which uses Cholesky decomposition to efficiently invert a symmetric matrix (Press et al. 2002).[10] This approach is considerably faster than the NUMPY least-squares package, both by eliminating NUMPY overheads and by using a faster method specifically appropriate for symmetric matrices. Since this approach to least-squares fitting uses vectorized functions and fast linear algebra operations, it is faster than other similarly accurate alternatives such as fitting a third-order Lagrange interpolating polynomial to four points of $s^2\xi(s)$, despite that this latter approach requires fewer evaluations of the correlation function.

As an alternative to the time-consuming determination of the polynomial coefficients, we determine c_n using a Taylor expansion in the cosmological parameters ($\Omega_{\rm m}$, $\Omega_{\rm b}$, $n_{\rm s}$, m_ν) centred on the fiducial cosmology. The dependence on σ_8 is straightforward, as it just rescales the polynomial coefficients by a multiplicative factor. This expansion assumes the mapping of parameters to power spectra appropriate for a νCDM cosmology; modifications to the transfer function, e.g. by warm dark matter or oscillations in the inflationary potential, will change this mapping and require fitting the polynomial coefficients rather than using the Taylor series.

To compute the Taylor expansion for each c_n, we first compute correlation functions and c_n for four cosmologies per parameter varied ($\Omega_{\rm m}$, $\Omega_{\rm b}$ $n_{\rm s}$, and m_ν): two with the parameter varied by $\pm1\sigma$ from the *Planck* 2018 best-fitting value (with $\sigma = 0.0056$, 0.001, and 0.0038, respectively) and two with the parameter varied by $\pm5\sigma$. For m_ν, where *Planck* provides only a 95 per cent upper limit of 0.12 eV, we use $m_\nu = 0$, 0.12, 0.18, and 0.24 eV as our test set (with $m_\nu = 0.06$ eV as our fiducial value). For each c_n and parameter p, we fit a line $c_n(p)$ with the intercept fixed to reproduce c_n in the fiducial cosmology. This allows us to achieve a good fit for a broad range of cosmologies away from the *Planck* best-fitting cosmology.

We must re-fit c_n at each z to ensure an accurate fit over most of the relevant range in scale (Section 2.2). Therefore, we must also determine the Taylor coefficients as a function of redshift. We measure the first-order Taylor coefficients for the three parameters for 60 sampling redshifts spaced at $\Delta z = 0.1$ between $z = 0$ and 6. We determine the Taylor coefficients at arbitrary z using a step function taking each z to the nearest $\Delta z = 0.1$ grid point less than z. We find that this method yields a sufficiently accurate $R_{\rm NL}$ (due to the relatively fine spacing in redshift) and is faster than linearly interpolating between redshifts.

Once the polynomial coefficients are fit, finding the non-linear scale is straightforward, requiring only algebraic operations. Nevertheless, we make a number of optimizations to the code implementing this. We store intermediate calculations to reduce computational expense, use only built-in PYTHON functions or functions from the MATH library, and use decimals rather than fractions wherever possible to avoid an additional division.

We compare the performance of our method to both a straightforward implementation of the standard method, using an adaptive quadrature numerical integration scheme to automatically ensure the error is within a given tolerance; and to an optimized calculation performing the integral using either the trapezoid rule or direct summation, with the sampling points pre-determined to maximize efficiency. The adaptive quadrature method is representative of standard methods for computing the non-linear radius in the literature; e.g. the CORE COSMOLOGY LIBRARY (Chisari et al. 2019)[11] uses the CQUAD routine in GSL, a doubly adaptive routine using Clenshaw–Curtis rules of increasing degree to calculate the integral at each level. We also compare to the trapezoid rule method to show that even with the fastest possible numerical integration settings for the standard method, our method is still faster.

For the standard method, evaluating the integral in Fourier space and obtaining $R_{\rm NL}$ via numerical root-finding, we use SCIPY.INTEGRATE.QUAD, SCIPY's adaptive integration routine wrapping the FORTRAN QUADPACK library. To maximize performance, we set the absolute and relative tolerances to 10^{-2}. We find that this yields $R_{\rm NL}$ accurate to better than 0.5 per cent. We do not find that transforming to an integral with finite bounds (i.e. via the transformation $kR = (1 + 1/t)^3$; Mead et al. 2015) improves performance.

In the optimized implementation of the standard method in Fourier space, we find that first-order summation is inaccurate and instead use the second-order trapezoid rule. We use 180 logarithmically spaced points between $k_{\rm min} = 10^{-3}$ h Mpc^{-1} and $k_{\rm max} = 10^4$ h Mpc^{-1} to compute the integral. As with fitting the polynomial coefficients, the scaling of the integral is relatively insensitive to the number of sampling points due to the vectorization of most operations. Therefore, our results will not change much if the number of sampling points changes.

For the optimized implementation of the configuration space integral (equation 7), we use 50 sampling points in y and pre-compute the kernel since it does not change from iteration to iteration of the root-finding. We evaluate the integral using direct summation over the 50 points in y. We find that this gives sufficient accuracy (better than 10^{-4}) and is considerably faster than second-order methods such as Romberg integration.

We use the SCIPY implementation of Newton's method to perform the root-finding. We perform the root-finding in log-space to prevent the root-finder from attempting to evaluate σ_R at negative R. We set the tolerance to 10^{-4}. We use this method because we find it to be the fastest and most robust for root-finding.

Finally, we make our PYTHON code publicly available at https://github.com/akrolewski/NonlinearMassFaster.

4 RESULTS AND DISCUSSION

We measure the accuracy of our algorithm for finding $R_{\rm NL}$ and σ_R compared to numerical integration of equation (9) using a large number of sampling points in k. We also measure the speed of our algorithm, both when we fit the coefficients c_n for every cosmology, and when we use a Taylor expansion to calculate c_n for cosmologies sufficiently close to *Planck* 2018. We compare the timing of our algorithm to optimized versions of the numerical integration and root-finding method in both configuration and Fourier space. We find the algebraic method is accurate to 0.1–1 per cent in mass and offers a factor of 20–60 speedup over the standard method for $R_{\rm NL}$, while the Taylor series method is accurate to 1–10 per cent

[10] http://www.netlib.org/lapack/

[11] https://github.com/LSSTDESC/CCL

Downloaded from https://academic.oup.com/mnras/article/500/4/4439/5989726 by guest on 24 April 2024

Table 1. Cosmologies used to test our method. The default cosmology is *Planck* 2018, and the cosmologies C1–C5 are chosen by randomly drawing Ω_m, σ_8 and n_s from a uniform distribution of width $\pm 2\sigma$ centred on the *Planck* 2018 values. m_ν is chosen uniformly between 0 and 0.18 eV (the 3σ limit on neutrino mass from *Planck*). Dashes indicate that a given parameter is unchanged from the row above. Accuracy and timing results for these cosmologies are given in Figs 5 and 6.

Name	σ_8	Ω_m	Ω_b	n_s	m_nu
$\sigma_8 + 0.06$	0.8702	0.3096	0.04897	0.9665	0.06
$\sigma_8 - 0.06$	0.7502	–	–	–	–
Planck 2018	0.8102	–	–	–	–
C1	–	0.3129	0.0490	0.9669	0.125
C2	–	0.3185	0.0498	0.9676	0.0515
C3	–	0.3145	0.0479	0.9616	0.0408
C4	–	0.3086	0.0507	0.9591	0.0992
C5	–	0.3004	0.0504	0.9663	0.130

in mass and 400–1000× faster than the standard method for R_NL. The applications described in Section 1 generally require better than 10 per cent accuracy on the non-linear mass, so the accuracy of our method is sufficient. We also find that our method computes $\sigma(R)$ 500× faster than the standard method for 100 sampling points in R, and to 1 per cent accuracy, sufficient to determine the mass function and the mass–bias relationship to <3 per cent. This is smaller than the uncertainty in the fitted relations of Tinker et al. (2008, 2010).

We use PYTHON 3.7.7, with NUMPY 1.18.5 and SCIPY 1.5.0. Timing tests are performed on a dual core 1.8 GHz Intel Core i5 processor.[12] We use seven cosmologies to test our method. We start with two where σ_8 is varied by ± 0.06 from its best-fitting *Planck* 2018 value, matching the tension between *Planck* and the low-redshift measurement from KiDS (Hildebrandt et al. 2020).[13] We also use five test cosmologies with Ω_m, Ω_b, and n_s drawn from a random uniform distribution between 2σ less than and 2σ greater than the *Planck* 2018 best-fitting value for each parameter. We also draw m_ν uniformly between 0 and 0.18 eV, corresponding to the 3σ upper limit on m_ν from *Planck*. These explore at a range in which many recent simulations lie (Klypin et al. 2016; Klypin & Prada 2018; Villaescusa-Navarro et al. 2020). The parameters for these test cosmologies are given in Table 1.

Our fiducial method, in which we re-fit the coefficients for each input power spectrum, is accurate to better than 0.3 per cent in R_NL (1 per cent in M_NL) at $0 < z < 6$ for all seven of these test cosmologies (Fig. 5). If we instead use a Taylor expansion about the *Planck* 2018 cosmology to generate the coefficients, the accuracy is somewhat worse, between 1 per cent and 10 per cent in mass. Therefore, the Taylor series method may be adequate at $z \sim 0$, where it offers 1 per cent accuracy in R_NL and 3 per cent accuracy in mass, but at higher redshifts it is likely best to explicitly re-fit the polynomial coefficients, depending on the accuracy demands of one's application.

We plot $R_\mathrm{NL}(z)$ in the left-hand panel of Fig. 5 for the *Planck* 2018 cosmology ($R_\mathrm{NL,fid}$) and for the two cosmologies with the largest deviation in $R_\mathrm{NL}(z)$, C5 and $\sigma_8 + 0.06$. At $z = 0$, R_NL in $\sigma_8 + 0.06$ (C5) is 7 per cent higher (8 per cent lower) than $R_\mathrm{NL,fid}$, increasing to 25 per cent higher (30 per cent lower) at $z = 6$. R_NL is very small at high redshift, with $R_\mathrm{NL}(z = 6) \approx 0.005\ h^{-1}$ Mpc. This does not imply that the $z = 6$ linear power spectrum is valid out to $k_\mathrm{NL} = 2\pi/0.005 \approx 1000\ h$ Mpc^{-1}. Rather, the k at which the linear and non-linear power spectra deviate is smaller than k_NL by a factor of a few.

Because we use R_NL in the *Planck* 2018 cosmology to set the fitting range, the accuracy of our method should degrade as the cosmology varies. However, for certain cosmologies and redshift ranges ($\sigma_8 - 0.06$ at $z < 4$, C2 at $z < 5$, and C1 and C3 at $z < 6$), the accuracy is *better* than the accuracy for *Planck* 2018. This is because the mismatch between R_NL in these cosmologies and $R_\mathrm{NL,fid}$ is actually beneficial, since the (cosmology-dependent) optimal upper bound is not exactly $1.9R_\mathrm{NL}$. For these cosmologies and redshifts, $1.9R_\mathrm{NL,fid}$ approaches the optimal upper bound at the points where the error approaches zero (e.g. $z \approx 4.2$ for C2).

The R_NL error for many of the test cosmologies increases at higher redshift. This is because R_NL is smaller at high redshift, and thus sensitive to the linear power spectrum at higher k where the power spectrum is more cosmology dependent.[14] This means that the disagreement between R_NL and $R_\mathrm{NL,fid}$ is larger, leading to a suboptimal fitting range and inaccurate polynomial coefficients. As a consequence, if we instead solve for the scale where $\sigma_R = 1$ (e.g. Norman 2010), our method will be more accurate because this scale is larger and less dependent on high k, yielding a better fitting range and more accurate polynomial coefficients.

We compare the timing for the algebraic method and the numerical integral plus root-finding method in both configuration and Fourier space (Fig. 6). If we fit the polynomial coefficients to the correlation function, our method is faster than the standard Fourier space method by 20–60×; if we generate the polynomial coefficients from a Taylor expansion about the *Planck* 2018 cosmology, our method is 400–1000× faster than the standard Fourier space method. For the algebraic method, this speedup also includes the fixed cost of transforming from $P(k)$ to $\xi(r)$, for which we use FFTLog to improve efficiency. Since the Taylor expansion method simply outputs the polynomial coefficients as a linear function of the cosmological parameters, it does not incur this extra cost, allowing it to be much faster than the algebraic method. The standard numerical integral plus root-finding method uses an adaptive integration scheme to ensure convergence on the numerical integrals. One could optimize for efficiency using a zeroth or first-order method (direct summation or trapezoid rule) with pre-determined sampling points. However, doing so would not be robust to variations in the input power spectrum.

The timing of the standard method has a slightly different redshift dependence than that of the algebraic method. The step features in Fig. 6 for the standard method arise from discrete changes in the number of steps needed to find R_NL. On the other hand, the timing of the algebraic method slightly improves with redshift, as at high z we fit fewer points to determine the polynomial coefficients.

Our method also allows faster calculation of the halo mass function and mass–bias relationship. Calculating $\sigma(R)$ is one of the major bottlenecks in this calculation, and our method greatly accelerates its computation compared to standard methods. Even for a single R, our method is faster than the standard method to compute $\sigma(R)$ using

[12] This is a similar architecture to the Cori Haswell nodes at the National Energy Research Supercomputing Center (NERSC) (see https://docs.nersc.gov/systems/cori/), hence the performance numbers outlined here can plausibly be scaled to get a rough estimate for the performance on a typical recent HPC system.

[13] Weak lensing measurements are sensitive to the parameter combination $S_8 = \sigma_8\sqrt{\Omega_\mathrm{m}/0.3}$. KiDS measures $S_8 = 0.737^{+0.040}_{-0.036}$ (Hildebrandt et al. 2020); if Ω_m is fixed to 0.3, this implies $\sigma_8 \sim 0.75$.

[14] Changing Ω_m and n_s tilts $P(k)$ with a pivot at $k \approx 0.1\ h$ Mpc^{-1}. Therefore, the linear power spectrum is more sensitive to the cosmological parameters at higher k.

Downloaded from https://academic.oup.com/mnras/article/500/4/4439/5989726 by guest on 24 April 2024

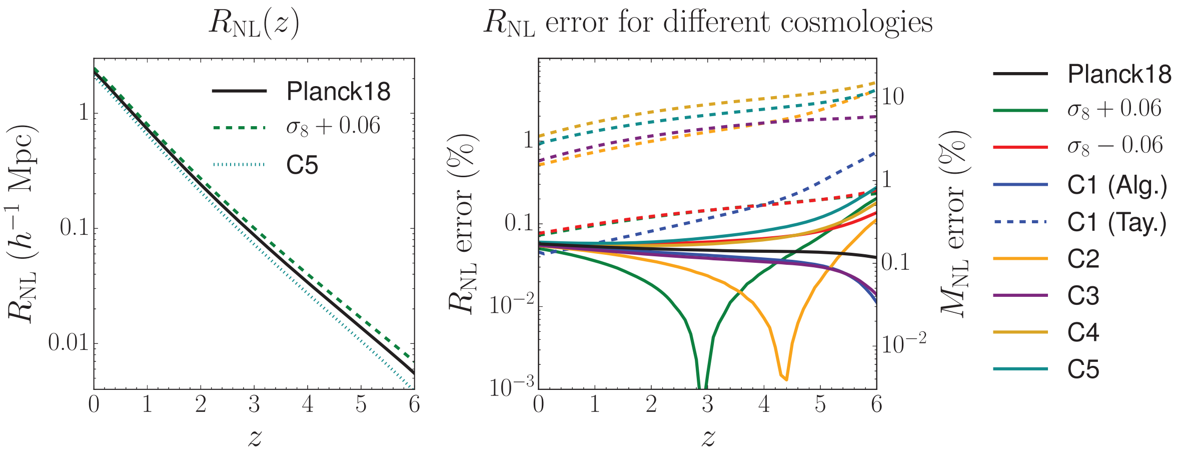

Figure 5. Left: $R_{\rm NL}(z)$ for the *Planck* 2018 cosmology (black), and the C5 and $\sigma_8+0.06$ cosmologies (dark cyan, dotted; green, dashed), which have the largest discrepancy with the *Planck* 2018 $R_{\rm NL}$. Right: Absolute value of the error on $R_{\rm NL}$ (left-hand vertical axis) and the non-linear mass (right-hand vertical axis; 3× the $R_{\rm NL}$ error) as a function of redshift. We compare the accuracy for our seven test cosmologies using the fiducial method, where we re-fit the coefficients to each cosmology (solid, coloured curves). We also show the Taylor series method, where we use a Taylor expansion about the *Planck* 2018 cosmology to generate the coefficients (dashed curves). Each colour stands for one of the seven test cosmologies, and the line style indicates whether we re-fit the coefficients or determine them from the Taylor series. Cosmological parameters are given in Table 1. At $z\sim 4.2$, the error on $R_{\rm NL}$ for C2 changes sign from positive to negative, leading to the zero-crossing feature in the golden curve (and likewise for the green curve at $z\sim 3$).

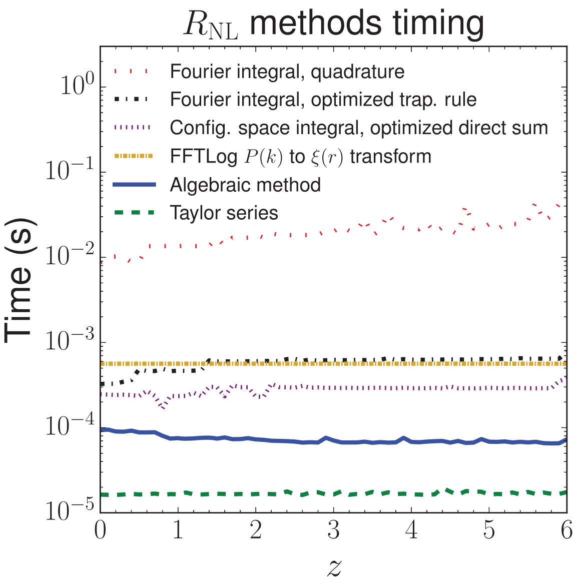

Figure 6. Comparison between the timing for our implementation of the algebraic method (solid blue) versus the standard method (vertical-dashed red). The standard method uses numerical integration with adaptive quadrature in Fourier space, plus root-finding. Optimized versions of the standard method are shown in dot-dashed black for the integral in Fourier space and in short-dashed red for the integral in configuration space. In yellow, we show the fixed cost of the FFTLog-based $P(k)$ to $\xi(r)$ transform (this line is constant in redshift because the $P(k)$ to $\xi(r)$ transform can be performed once for all redshifts). We also show the timing of our method if we instead use a Taylor expansion to generate the coefficients rather than fitting directly to the correlation function (long-dashed green; bottom-most curve). The algebraic method is 20–60× faster than the standard method with the integral in Fourier space (100–300× faster excluding the time for the $P(k)$ to $\xi(r)$ transform). The 20–60× speedup compares the sum of the solid blue and very short-dashed golden lines to the short-dashed red line. The Taylor series method is 400–1000× faster. The algebraic method is still 3–10× faster than the standard method with simple integration rules (trapezoidal or direct sum) and sampling points optimized for efficiency (excluding the fixed cost of the $P(k)$ to $\xi(r)$ transform).

a numerical integral with adaptive quadrature. The standard method takes 3.7×10^{-3} s per evaluation on our test hardware, whereas our method takes 1.4×10^{-4} s per evaluation (using the piecewise polynomial fit to $\xi(s)$ with $R_{\rm max,1}=30$ h^{-1} Mpc and $R_{\rm max,2}=2$ h^{-1} Mpc). Our method also must transform from $P(k)$ to $\xi(r)$, which takes 5.6×10^{-4} s; therefore, for a single R or halo mass, our method is 5× faster than the standard method.

However, one often desires the mass function or bias at many different halo masses. Our method scales much better than the standard method, since each additional point in R or halo mass requires only a few algebraic evaluations rather than another numerical integral. Therefore, our method is ∼500× faster than the standard method to compute the halo mass function or bias at 100 points in mass. We even find that the optimized trapezoid-rule Fourier space integral (with no automatic error calculation or convergence testing), which is the fastest possible integration method in Fourier space, is 8× slower than our method for 100 sampling points. Therefore, our method provides a considerable speedup for the halo mass function and mass–bias relation by avoiding numerical integrals.

5 CONCLUSIONS

The non-linear mass is the characteristic scale of halo formation, defined as the scale on which σ_R, the rms of the density field inside a sphere of radius R, reaches the linear threshold for spherical collapse, $\delta_{\rm c}=1.686$. We present a method to accelerate computation of the non-linear mass by an order of magnitude by fitting a polynomial to the correlation function and evaluating σ_R in configuration space. Our method can be further accelerated by another order of magnitude by using a Taylor series about the *Planck* 2018 cosmology for the correlation function fitting coefficients. Our method also allows for very fast repeated calculations of $\sigma(R)$ in mass function and mass-bias calculations, enabling a speedup of 500× for 100 sampling points in halo mass. Since nearly all of the evaluation time of our method is in fixed costs, the speedup factor grows as the number of sampling points is increased. We make our PYTHON implementation publicly available at https://github.com/akrolewski/NonlinearMassFaster.

Downloaded from https://academic.oup.com/mnras/article/500/4/4439/5989726 by guest on 24 April 2024

Overall, our method is sufficiently accurate for future applications, with accuracy in the non-linear mass generally exceeding 1 per cent at $z < 6$ for a variety of cosmologies. The error on the halo mass function and mass–bias relation from our method is much smaller than the statistical scatter on these quantities in Tinker et al. (2008, 2010). The accuracy is better at lower redshift, where $R_{\rm NL}$ is larger and thus depends on the power spectrum at lower k, where it is less sensitive to cosmological parameters.

A fast and accurate method to compute non-linear mass will enable repeated calculations of the non-linear mass. This is useful for a number of areas in cosmology, including dark matter halo profiles and shapes, shape of the scale-dependent bias, and halo model calculations. Other extensions of our method are also possible: while we accelerate the computation of the variance of the density field in this paper, we could also potentially apply this method to higher cumulants of the density field as well.

ACKNOWLEDGEMENTS

The authors thank the referee, Alexander James Mead, for a very thorough and helpful referee report and suggestions that have greatly improved the paper. AK thanks Antony Lewis for insight into the high-k linear power spectrum. ZS thanks Hillary Child for bringing this problem to his attention and for useful input on this project. ZS is also grateful to both Lawrence Berkeley National Laboratory and the Berkeley Center for Cosmological Physics for hospitality during this work.

DATA AVAILABILITY

No new data were generated or analysed in support of this research. The code is publicly available at https://github.com/akrolewski/NonlinearMassFaster.

REFERENCES

Abazajian K. et al., 2005, ApJ, 625, 613
Bernardeau F., Colombi S., Gaztañaga E., Scoccimarro R., 2002, Phys. Rep., 367, 1
Bocquet S. et al., 2019, ApJ, 878, 55
Bryan G. L., Norman M. L., 1998, ApJ, 495, 80
Bullock J. S., Kolatt T. S., Sigad Y., Somerville R. S., Kravtsov A. V., Klypin A. A., Primack J. R., Dekel A., 2001, MNRAS, 321, 559
Castorina E., Sefusatti E., Sheth R. K., Villaescusa-Navarro F., Viel M., 2014, J. Cosmol. Astropart. Phys., 2014, 049
Castorina E., Carbone C., Bel J., Sefusatti E., Dolag K., 2015, J. Cosmol. Astropart. Phys., 2015, 043
Cataneo M., Emberson J. D., Inman D., Harnois-Déraps J., Heymans C., 2020, MNRAS, 491, 3101
Child H. L., Habib S., Heitmann K., Frontiere N., Finkel H., Pope A., Morozov V., 2018, ApJ, 859, 55
Chisari N. E. et al., 2019, ApJS, 242, 2
Costanzi M., Villaescusa-Navarro F., Viel M., Xia J.-Q., Borgani S., Castorina E., Sefusatti E., 2013, J. Cosmol. Astropart. Phys., 2013, 012
Dalal N., White M., Bond J. R., Shirokov A., 2008, ApJ, 687, 12
Eke V. R., Cole S., Frenk C. S., 1996, MNRAS, 282, 263
Gunn J. E., Gott J., Richard I., 1972, ApJ, 176, 1
Hahn O., Porciani C., Carollo C. M., Dekel A., 2007a, MNRAS, 375, 489
Hahn O., Carollo C. M., Porciani C., Dekel A., 2007b, MNRAS, 381, 41
Hamilton A. J. S., 2000, MNRAS, 312, 257
Harikane Y. et al., 2018, PASJ, 70, S11
Hildebrandt H. et al., 2020, A&A, 633, A69
Howlett C., Lewis A., Hall A., Challinor A., 2012, J. Cosmol. Astropart. Phys., 1204, 027
Hu W., Eisenstein D. J., 1998, ApJ, 498, 497
Hu W., Sugiyama N., 1996, ApJ, 471, 542
Jing Y. P., Suto Y., 2002, ApJ, 574, 538
Jose C., Lacey C. G., Baugh C. M., 2016, MNRAS, 463, 270
Jose C., Baugh C. M., Lacey C. G., Subramanian K., 2017, MNRAS, 469, 4428
Kaiser N., 1986, MNRAS, 222, 323
Klypin A., Prada F., 2018, MNRAS, 478, 4602
Klypin A., Yepes G., Gottlöber S., Prada F., Heß S., 2016, MNRAS, 457, 4340
Kravtsov A. V., Borgani S., 2012, ARA&A, 50, 353
Lacey C., Cole S., 1993, MNRAS, 262, 627
Lewis A., Challinor A., Lasenby A., 2000, ApJ, 538, 473
Li Y., 2019, mcfit: Multiplicatively Convolutional Fast Integral Transforms. Astrophysics Source Code Liabrary, record ascl:1906.017
Ma C.-P., Fry J. N., 2000, ApJ, 543, 503
Mead A. J., 2017, MNRAS, 464, 1282
Mead A. J., Peacock J. A., Heymans C., Joudaki S., Heavens A. F., 2015, MNRAS, 454, 1958
Nakamura T. T., Suto Y., 1997, Prog. Theor. Phys., 97, 49
Norman M. L., 2010, preprint (arXiv:1005.1100)
Oguri M., Takada M., Umetsu K., Broadhurst T., 2005, ApJ, 632, 841
Planck Collaboration VI, 2020, A&A , 641, A6
Press W. H., Teukolsky S. A., Vetterling W. T., Flannery B. P., 2002, Numerical Recipes in C++ : The Art of Scientific Computing, 2nd edn. Cambridge Univ. Press, New York
Seljak U., Warren M. S., 2004, MNRAS, 355, 129
Seljak U. et al., 2005, Phys. Rev. D, 71, 043511
Tinker J., Kravtsov A. V., Klypin A., Abazajian K., Warren M., Yepes G., Gottlöber S., Holz D. E., 2008, ApJ, 688, 709
Tinker J. L., Robertson B. E., Kravtsov A. V., Klypin A., Warren M. S., Yepes G., Gottlöber S., 2010, ApJ, 724, 878
Umetsu K. et al., 2020, ApJ, 890, 148
Villaescusa-Navarro F., Marulli F., Viel M., Branchini E., Castorina E., Sefusatti E., Saito S., 2014, J. Cosmol. Astropart. Phys., 2014, 011
Villaescusa-Navarro F. et al., 2020 ApJS, 250, 2
Wechsler R. H., Bullock J. S., Primack J. R., Kravtsov A. V., Dekel A., 2002, ApJ, 568, 52
Zehavi I. et al., 2005, ApJ, 621, 22

This paper has been typeset from a TEX/LATEX file prepared by the author.

Downloaded from https://academic.oup.com/mnras/article/500/4/4439/5989726 by guest on 24 April 2024